GEOPHYSICS, VOL. 72, NO. 1 (JANUARY-FEBRUARY 2007); P. V1–V11, 16 FIGS.
10.1190/1.2374799

Adaptive wavelets for analyzing dispersive seismic waves

A. Kritski[1], A. P. Vincent[2], D. A. Yuen[3], and T. Carlsen[4]

ABSTRACT

Our primary objective is to develop an efficient and accurate method for analyzing time series with a multiscale character. Our motivation stems from the studies of the physical properties of marine sediment (stiffness and density) derived from seismic acoustic records of surface/interface waves along the water-seabed boundary. These studies depend on the dispersive characteristics of water-sediment surface waves. To obtain a reliable retrieval of the shear-wave velocities, we need a very accurate time-frequency record of the surface waves. Such a time-frequency analysis is best carried out by a wavelet-transform of the seismic records. We have employed the wavelet crosscorrelation technique for estimating the shear-wave propagational parameters as a function of depth and horizontal distance. For achieving a greatly improved resolution in time-frequency space, we have developed a new set of adaptive wavelets, which are driven by the data. This approach is based on a Karhunen-Loeve (KL) decomposition of the seismograms. This KL decomposition allows us to obtain a set of wavelet functions that are naturally adapted to the scales of the surface-wave modes. We demonstrate the superiority of these adaptive wavelets over standard wavelets in their ability to simultaneously discriminate the different surface-wave modes. The results can also be useful for imaging and statistical data analysis in exploration geophysics and in other disciplines in the environmental sciences.

INTRODUCTION

Our basic motivation in this study comes from imaging seismic surface waves propagating along the water-seabed interface. These surface-wave studies are well established and are for the purpose of retrieving physical properties of inhomogeneous sediments lying between the ocean, a fluid layer, and the solid substrate (Biot, 1952; Haskell, 1953; Poiree and Luppe, 1991; Aki and Richards, 2002). Because surface-wave velocities are directly related to the shear modulus as a function of the depth and distance from the receiver (Haskell, 1953), this allows us to study the physical properties of marine sediments remotely by measuring the dispersive properties of surface waves. The directly measured group and phase velocities of different surface-wave modes are further used to invert for the shear-wave velocities as a function of both depth and horizontal distances (Haskell, 1953; Strick, 1959; Hovem et al., 1990; Gaiti et al., 1994; Kuperman et al., 2000; Potty et al., 2003).

We consider the problem of the accurate separation of surface-wave dispersive modes. This is important in the inversion for the shear properties (Gaiti et al., 1994). Surface-wave modes with different horizontal wavenumbers, and therefore, different frequencies, would arrive at the receiver at different times, depending on the dispersion relationship between group and phase velocities and frequency. Solving the mode separation problem requires an extremely accurate analysis of their propagational parameters in the time-frequency plane. Therefore, first of all, seismic records have to be translated into time-frequency space. Traditional methods (Bendat and Piersol, 1980; Priestley, 1981), such as Fourier analysis, spatial- and time-correlation functions, stochastic estimations, and the Gabor transform do not provide a high-quality image of the surface wave that would be sufficient for a reasonable separation of the various modes. In this study, we use the techniques of wavelet transform (Kaiser, 1994) to decompose the surface-wave records into the time-frequency plane (Kritski et al., 2002a, b).

Wavelets (Goupillaud et al., 1984; Grossmann and Morlet, 1984; Daubechies, 1992; Holschneider, 1995) represent a powerful mathematical tool, which can efficiently separate out one-dimensional multiscale signals over the time-space/frequency plane. Wavelet analysis has proven its prowess in decomposing seismic waves into

Manuscript received by the Editor August 22, 2005; revised manuscript received August 18, 2006; published online November 16, 2006.
[1]Statoil Research Centre, Arkitekt Ebbellsvei 10, Rotvoll, N-7005 Trondheim, Norway. E-mail: akr@statoil.com.
[2]Université de Montréal, Département de Physique, C. P. 6128, Succ., Centre-Ville, Montreal, QC, H3C 3J7, Canada. E-mail: vincent@astro.umontreal.ca.
[3]University of Minnesota, Minnesota Supercomputing Institute, Department of Geology and Geophysics, Minneapolis, Minnesota 55455. E-mail: daveyuen@gmail.com.
[4]Formerly Norwegian University of Science and Technology, Department of Electronics and Telecommunications, Trondheim, Norway; presently CGG-Marine, Postboks 243, O. H. Bangs vei 70, N-1322 Høvik, Norway. E-mail: trygvegu@hotmail.com.

time and period (frequency) representations (Chui, 1992; Coifman et al., 1992; Kaiser, 1994; Holschneider, 1995; Kumar and Foufoula-Georgiou, 1997; Mallat, 2001; Yuen et al., 2002; Kritski et al., 2002a, b; Yuen et al., 2004; Bodet et al., 2005). However, we can greatly improve the resolution by using a novel class of wavelets that is better suited for the geophysical situation in marine sedimentary environments than standard wavelets, such as Morlet-wavelets (Goupillaud et al., 1984). This is our basic goal, to construct a set of adaptive wavelets directly from the available seismic records. Our approach is based on performing the Karhunen-Loeve (KL) (Karhunen, 1947; Loeve, 1955) decomposition of seismic records. From this decomposition, we obtain a set of wavelet functions that are naturally adapted to the given multiscale signals. We will demonstrate this approach on selected synthetics and on sampled records of the seismic surface wave propagating in marine sediments. We will show that the developed adaptive wavelets discriminate various features in complex multiscale signals better than standard wavelets, such as Morlet wavelets, which are in common use in general geophysics (Chui, 1992) or in geophysical marine exploration (Kumar and Foufoula-Georgiou, 1997).

WAVELET TRANSFORM

Different methods are used in signal processing for displaying time series in time-frequency space. The most common methods include moving-window filtering based on the Gabor matrix representation (Gabor, 1946; Dziewonski et al., 1969; Haykin, 1991; Yuen et al., 2002); Wigner-Ville distribution (Haykin, 1991; Hogan and Lakey, 2005), which was successfully used in optical signal processing; and the wavelet transform (Goupillaud et al., 1984; Grossmann and Morlet, 1984; Holschneider et al., 1989; Daubechies, 1992; Kaiser, 1994; Holschneider, 1995; Mallat, 2001). The continuous wavelet transform overcomes traditional time-frequency resolution problems and, perhaps, represents the most balanced tack for decomposing multiscale signals into time-frequency space. In our previous studies (Kritski et al., 2002a, b), we have employed the continuous wavelet transform. Wavelet transform $W_f(b,a)$ of a time-dependent function $f(t)$ at time b relative to the wavelet basis function $\psi(t)$ at frequency scale $1/a$ (Holschneider, 1995) is given by

$$W_f(b,a) = \frac{1}{\sqrt{a}}\int_{-\infty}^{+\infty} f(t)\overline{\psi\left(\frac{(t-b)}{a}\right)}dt, \qquad (1)$$

where b has the dimension of time and $1/a$ is the frequency.

We can make use of this family of functions by adapting them naturally to multiscale signals. We will demonstrate this property by using an example drawn from seismic wave propagation, as recorded on seismograms.

METHOD FOR CONSTRUCTING ADAPTIVE WAVELETS

The technique for determining the most suitable wavelets is based on the search for correlation in the patterns of oscillations in a set of time records. The time series is assumed to have a zero mean. First, we form a covariance matrix $\boldsymbol{\phi}(\mathbf{x},\mathbf{x}')$, where $\mathbf{x}$ and $\mathbf{x}'$ are in time, from the cross-lag correlation matrix with the minimum time lag taken to be the sampling interval. This matrix is then decomposed into orthogonal components with the Karhunen-Loeve (KL) method, also known as the Orthogonal Decomposition Theorem or Principal Component Analysis (PCA) (Karhunen, 1947; Loeve, 1955; Golub and Van Loan, 1983; Riesz and Nagy, 1955; Aster et al., 2005). This approach has proven to be very useful in climate dynamics and other areas (Vautard and Ghil, 1989; Yiou et al., 2000). Our choice of the KL transform is based on the concept of minimizing the average approximate error according to the L_2 norm. When one projects discrete signal $f(i):i = 1,N$ with size n onto first M vectors of the orthogonal basis $\beta = \{\psi_m\}$, $0 < m < N$, the average approximation error is

$$\epsilon[M] = E[|f - f_M|^2] = \sum_{m=M}^{N-1} E[|\langle f, \psi_m\rangle|^2]. \qquad (2)$$

Quantities inside the angled brackets are averaged over the time window. Mallat (2001) has proved that the basis that minimizes the average linear approximation error is exactly the Karhunen-Loeve basis set, which diagonalizes the covariance matrix of the signal $f(i)$. Here we extend this applicability to investigate surface-wave modes. Below, we briefly summarize the method for time-discrete signals by extending the formalism for a set of time series.

The first step in this KL-based wavelet transform is an estimate of the covariance matrix. Reference papers on this topic include Helstrom (1968), Packard et al. (1980), Vautard and Ghil (1989), Gibson et al. (1992), and Yiou et al. (2000).

For an input with single time-discrete signals $x_i = x(i\Delta t)$, for $0 < i < N$, (N is the number of samples), by forming a delay matrix $\mathbf{X}_i(t)$ whose columns are lag-shifted elements of x_i (Packard et al., 1980; Broomhead and King, 1986; Gibson et al., 1992), we can denote the covariance matrix as

$$\boldsymbol{\phi}(\mathbf{x},\mathbf{x}') \equiv \boldsymbol{\phi}(\mathbf{x}_i,\mathbf{x}_j) = \mathbf{X}(t)_i^T\mathbf{X}(t)_j = \langle \mathbf{x}_i(t)\mathbf{x}_j(t)\rangle, \qquad (3)$$

For each record, we deal only with the elements of the covariance matrix and form the autocorrelation matrix:

$$\mathbf{A}(\tau) = (2T)^{-1}\lim_{T\to\infty}\int_{-T}^{+T} x(t)x(t-\tau)dt, \qquad (4)$$

where T is the time interval over which we consider our time series. Lag time τ is set as an integer multiple of the sampling time (Δt): $\tau = h\Delta t$.

We assume that time realization $N\Delta t$ is large enough to be considered an effective infinite time average. In this case, $\boldsymbol{\phi}(\mathbf{x},\mathbf{x}')$ in equation 3 approaches the autocorrelation matrix.

One can now solve an eigenvalue problem in terms of the covariance matrix. This matrix is real and symmetric and, therefore, it has always an eigenvector solution (Golub and Van Loan, 1983; Aster et al., 2005). A spectrum can be defined in terms of the eigenvalues. We can write (Golub and Van Loan, 1983; Aster et al., 2005) the following eigenvalue problem for $|\lambda_i|^2$:

$$\int \boldsymbol{\phi}(\mathbf{x},\mathbf{x}')\boldsymbol{\psi}_i(\mathbf{x}')d\mathbf{x}' = |\lambda_i|^2\boldsymbol{\psi}_i(\mathbf{x}), \qquad (5)$$

where i represents the index for the lag, and $\boldsymbol{\psi}_i$ represents the eigenvectors. The eigenvalues $|\lambda_i|^2$ define the eigenspectrum (Golub and Van Loan, 1983; Aster et al., 2005). The eigenvectors $\boldsymbol{\psi}_i(\mathbf{x})$ represent the oscillatory modes.

The eigenvectors $\boldsymbol{\psi}_i(\mathbf{x})$, ordered by their corresponding positive eigenvalues (arranged in the descending fashion: $\lambda_1 \geq \lambda_2 \geq \cdots \geq \lambda_k \geq \lambda_M \geq 0$), provide an orthogonal basis for expanding the time series x_i with respect to the chosen time-lagged series $M(M \leq N)$. The principal components z_m are found by the expansion:

$$z_m(t) = \sum_{i=1}^{M} [x_i(t)\,\psi_i \sqrt{|\lambda_i|^2}]. \tag{6}$$

They represent the projections of the delay vectors into the eigenvectors. The set of principal components z_m provides full reconstruction of the input time series from its eigenvalues and eigenvectors.

Vautard and Ghil (1989) and Yiou et al. (2000) proposed an extension of the eigenspectrum analysis method to rectangular matrices called the singular-spectrum analysis (SSA) (Golub and Van Loan, 1983). They applied this SSA method to modulate a predefined set of time windows. The number of window functions was proportional to the order M of the autocorrelation matrix. This type of sliding window provides a local SSA with different scale analysis of the input signal. Furthermore, Yiou et al. (2000) pointed out the similar oscillatory properties of the continuous wavelet-transform derivatives and the eigenfunctions set (eigenvectors multiplied with corresponding eigenvalue) obtained in SSA at each window size M. They propose to consider the eigenfunctions as a new set of wavelet functions derived from the data.

Based on this concept, we have developed a new approach to construct a family of wavelet functions. In contrast with the method of Vautard and Ghil (1989) and of Yiou et al. (2000), we use the entire data set to solve the large eigenvalue problem, $M = N$.

We can further rewrite equation 6 as

$$z_m(t) = \sum_{i=1}^{N} [x_i(t)\,\psi_i \sqrt{|\lambda_i|^2}]. \tag{7}$$

These eigenvectors, multiplied with corresponding eigenvalues, form eigenfunctions, which include all possible scales in the given data record. They define the complete solution to the eigenvalue problem for the given data set:

$$\xi_m(t) = \sum_{i=1}^{N} \psi_i \sqrt{|\lambda_i|^2}. \tag{8}$$

We use these eigenfunctions as basis functions to form a new wavelet set. At the next step, we will design a new set of wavelet functions from an orthogonal set of the eigenfunctions (equation 8).

Normally, a procedure for designing a new wavelet set would include shifting and scaling of a single prototype wavelet called a mother wavelet. This produces a set of daughter wavelets carrying the rescaled shape of the mother wavelet. In our approach, we use a different concept: Each of the obtained eigenfunctions has a unique shape and frequency content. Together, all of the obtained eigenfunctions define the variability of all possible time scales in the signal, and they are sufficiently complete to reconstruct the input signal. We use all the eigenfunctions as a prototype set for constructing a new wavelet set. Each of these eigenfunctions is kept without rescaling. From this basis, we design the new wavelet functions.

A wavelet function is defined as an oscillating function localized both in frequency and time (Kaiser, 1994). If a wavelet function is decaying in time over some maximum, this maximum would define the wavelet's localization in time. The frequency of the oscillation is the wavelet's localization in frequency. In other words, the wavelet basis should have support in time and frequency. The temporal width (support) of the wavelet's functions is not constant; it varies for each wavelet function. The frequency band support varies as well, proportionally to 1/(time support).

Each eigenfunction provides a frequency localization that is perfectly adapted to the variety of the scaled oscillations in the given time record. These functions are orthogonal (they provide full reconstitution of the input signal similar to the Fourier analysis) and are suitable as an analyzing tool to search for the scales (frequencies) in the time record, for example, as an SSA method. However, these functions are not localized in time, i.e., they are not wavelet functions. Thus, the decomposition over the frequency-time plane is not possible yet. We apply windowing in the time domain to each eigenfunction (equation 8) in order to achieve localization in time.

Every wavelet function is generated by multiplying a window and an eigenfunction in the time domain. The width of the window is unique for each eigenvector, and it is defined as the result of the trade-off between frequency and time support, as it is restricted by the Heisenberg uncertainty principle (Harris, 1978; Priestley, 1981; Mallat, 2001).

High- and low-frequency eigenfunctions need different time and frequency support. High-frequency eigenfunctions require a smaller time interval as the scales (periods) they contain are smaller. Thus, a proper window function should provide small time support for high-frequency eigenfunctions, and increases when analyzing eigenvectors have low frequencies (Kaiser, 1994; Mallat, 2001).

New wavelet functions (windowed eigenvector functions) can be expressed mathematically as

$$\zeta_i(t) = \frac{\xi_i(t)\,\nu(l_i)}{\|\xi_i(t)\,\nu(l_i)\|_2}, \tag{9}$$

where $\xi(t)$ is a basic eigenfunction, $\nu(l_i)$ is a window function of length l_i and $\|\ldots\|_2$ is the L_2-norm.

Finally, we can write a set of new wavelet functions as

$$\zeta_m(t) = \sum_{i=1}^{N} \frac{\xi_i(t)\,\nu(l_i)}{\|\xi_i(t)\,\nu(l_i)\|_2}. \tag{10}$$

The shapes of the new wavelet functions are derived from the data directly and they are unique. Each new wavelet function is defined from the corresponding eigenfunction but not from dilation and translation of the same eigenfunction. The wavelet functions obtained in this manner describe the largest possible variability of scales in the data record.

The wavelet design procedure should be accomplished with the orthogonality test for the obtained wavelet functions, and the wavelet functions should also satisfy the admissibility condition (Kaiser, 1994; Mallat, 2001). The optimal solution for time windowing would include the conservation of orthogonality of the obtained wavelet functions basis. We note that not all time-windowing would necessarily preserve the orthogonality of the windowed eigenfunctions. If the windowing does not preserve the orthogonality, an additional orthogonalization should be applied to the windowed eigenvectors to ensure that the resultant set of basis functions is orthogonal. Some comments on the windowing in the wavelet design are included in the section below entitled, "Choice of the optimal window."

The last wavelet property we would like to discuss here is an optimization of the obtained wavelet set in terms of producing the maximum number of nonzero wavelet coefficients. The properties of the wavelet that mostly influence the number of nonzero coefficients are the following: regularity of the wavelet function, number of vanishing moments of the wavelet, and its temporal support.

Wavelets are considered to be optimal when they have the minimum support size with the largest possible number of vanishing moments (for example, Daubechies wavelets). The number of vanishing moments mostly affects the number of nonzero wavelet coefficients (Abbate et al., 2002). We do not use scaling functions in our wavelet design; however, a temporal support in our case is defined by the window function $\nu(l_i)$, whose length is a subject of optimization. An optimal solution would include a trade-off between the window type, size (support), and number of the vanishing moments of the windowed eigenfunction to produce a maximum number of nonzero coefficients. There exist various ways for solving this type of optimization problem, for example, Abbate et al. (2002) analyzed differentiability properties of the Fourier transform of the wavelet functions. The problem of a different kind arises when dealing with adaptive wavelets based on the eigenfunctions derived from complex multiscale seismic signals. These eigenfunctions might have a frequency content that has a limited bandwidth, i.e., it is not just one isolated frequency. Each eigenfunction has its own frequency signature. By reducing the temporal support when applying a nonoptimized window, we can cut off some relevant higher frequencies. Each eigenfunction, in this case, needs an individual windowing procedure. We do not yet have an optimal solution for this problem.

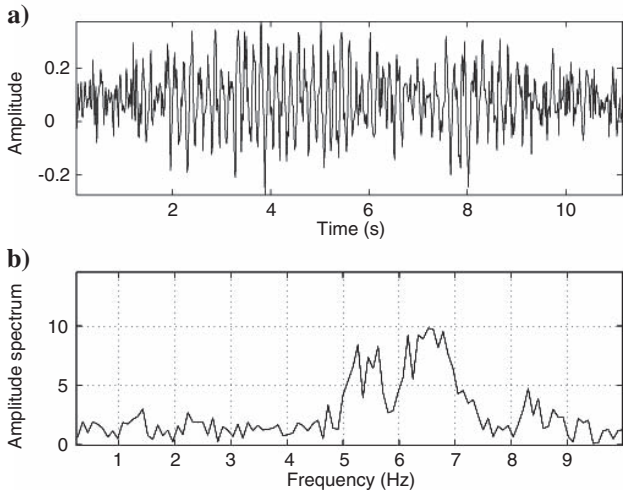

Figure 1. (a) Time representation of the field seismic record signal with two modes or events. (b) The associated frequency spectrum.

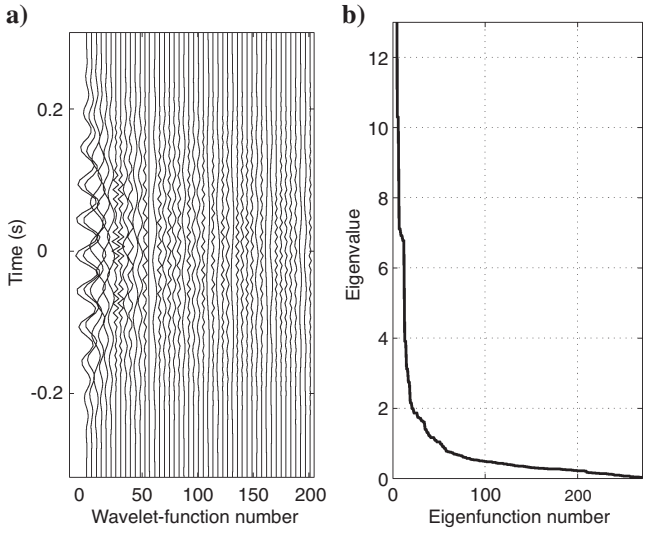

Figure 2. Selected adaptive modes. (a) The first 200 modes (each fifth mode) corresponding to the most powerful components of the KL transform of the seismic record in Figure 1. (b) Eigenspectrum of the input signal. The eigenvalues set is performed in a descending order. The eigenvalues are multiplied with the corresponding eigenfunctions from the resulting eigenset, or eigensolution, for the given data set.

We illustrate here the adaptive wavelet design procedure for a time seismic record that contains a surface-wave arrival of two events (surface-wave modes) (Figure 1). First, we display the spectrum of the eigenvalues in the descending order. These eigenvalues are displayed in Figure 2b. This type of ordering places the most coherent signal patterns at the beginning of the singular spectrum and the noncoherent set at the end of the spectrum. First (about 40) values of the eigenspectrum multiplied with the first 40 eigenfunctions define the components that yield the biggest contribution to the input signal. The rest of the eigenspectrum represents, in fact, incoherent noise, which plays a small role in constituting the original signal and, from the statistical point of view, can be neglected; although for the full representation of the signal, it is necessary to keep all components to be able to reconstruct the original signal.

For constructing the adaptive wavelets, we then weight the obtained eigenvectors with a weight given by the corresponding eigenvalue. At the next stage, we require that the weighted eigenvectors (eigenfunctions) have a compact support or that they sufficiently decay in time to obtain good localization in time and frequency. For this particular case, the following simple window implementation has been applied:

$$l = \left[\frac{N}{\log_2(k)} \right], \tag{11}$$

where $k = \left(\frac{f_i}{f_s} N\right)$, l is the window width, N is the number of samples, f_i is the representative frequency of the ith eigenfunction, and f_s is the sampling frequency of the input signal.

The adaptive-wavelet functions obtained (selected for illustration purposes as each fifth function) are displayed in time in Figure 2a.

Finally, after the adaptive-wavelet transform has been applied to the original signal, we then construct a time-frequency image by sorting out the wavelet-transform amplitudes (moduli) for the frequency components.

The moduli of the adaptive-wavelet transform applied to decompose the original signal are shown in Figure 3a.

We would like now to demonstrate that the number of wavelet functions involved in the adaptive-wavelet transform can influence the quality of the image. We present here the results of the adaptive-wavelet transform of the signal (Figure 1a) with only the first 40 values and with 10 wavelet functions. In this way, the first 40 eigenvectors shown in Figure 3b represent the components that would yield the largest contribution to the input signal. The image quality of the two events seen in the time-frequency plots remains almost the

same, with no noticeable distortions in their shapes. At the same time, it is clear that the image looks much more free from noise. By cutting part of the eigenspectrum with large numbers, we reduced the incoherent noise components without distorting the signal time-frequency representation, and significantly lowered computation costs.

Figure 3c represents the time-frequency amplitudes after applying the adaptive wavelet where the first 10 eigenfunctions were taken into consideration. The image quality of the events is obviously unacceptable. Only one event could be clearly identified, although its shape is significantly distorted. Neglecting the energetically valuable eigenfunction results in poor imaging. On the other hand, dropping the eigenfunction with large magnitude in the eigenspectrum could help us to suppress the incoherent noise in the final image. We note that, for the full representation of the original signal, it is necessary to retain all of the eigenfunctions. In this case, we have verified the Parseval equality (Torrence and Compo, 1998; Abbate et al., 2002) for these adaptive wavelets.

A similar consideration can be made of continuous wavelet transform. Orthogonal wavelets keep the proportion between the number of convolutions at each scale and the width of the wavelet base at that scale (Torrence and Compo, 1998). This gives a complete and most compact representation of the signal but not a smooth one in terms of spectral amplitudes: a wavelet spectrum would have a block-wise structure. By limiting the number of scales or changing the nondimensional angular frequency in the continuous wavelet transform, one can provide a smoother amplitude distribution and, thus, improve the wavelet image quality where a fine variation of amplitude is important. However, in this case it would not be possible to reconstruct the original signal from its wavelet transform. An example of this type of smoothing of the continuous wavelet transform can be found in Appendix A and in Figure A-4b, where, by limiting Morlet wavelet scales, a smoother image has been obtained.

Generalization of this approach to rectangular matrices is quite straightforward by following the singular-value decomposition formalism (Aster et al., 2005).

METHOD IMPLEMENTATION ON SEISMOGRAMS

Using the above idea, we now look for the possibility of a simultaneous time-frequency analysis of a set of surface-wave records. We use only one time window for $M = N$ (number of samples), i.e., all the data. We then consider P seismic records:

$$x_j(i\Delta t) \quad (i = 1,N;\ j = 1,P). \tag{12}$$

First, we find the delay matrix for each record, and then we find the set of crosscorrelation functions:

$$K_{lk} = X_l^T X_k, \tag{13}$$

where l and k are the indices for different station records.

For $l = k$, we arrive at the autocorrelation function. Thus, we can form a global covariance matrix $\mathbf{K}$, where each element represents a crosscorrelation matrix for all of the data records:

$$\mathbf{K}_{lk} = \begin{pmatrix} K_{11} & K_{12} & \dots & K_{1P} \\ \dots & & & \dots \\ K_{P1} & K_{P2} & \dots & K_{PP} \end{pmatrix}. \tag{14}$$

Next, we compute the eigenvectors and eigenvalues $\{\psi_{ij}, \lambda_{ij}\}$ for each element (or block) of the global matrix $\mathbf{K}_{lk}$, where $i,j:i = 1,N$; $j = 1,N$; are indices representing time, and $k,l:k = 1,P$; $l = 1,P$; are indices associated with the record number. The computed eigenfunctions for all blocks form an eigenvalue solution to the global matrix $\mathbf{K}_{lk}$.

The eigenfunctions, obtained in this manner, describe the largest possible variability of scales in the data records. These eigenfunctions reflect the complexity of the surface-wave behavior to the entire extent. This approach would allow the imaging of the surface-wave modes from the whole data set. This imaging would potentially contain all information of the most relevant scales in the seismic data over the whole study area; these scales can be inverted later for the physical properties of marine sediments over large distances.

CHOICE OF AN OPTIMAL WINDOW

We have generated each wavelet function by multiplying a window with the eigenfunction in the time domain. The length of this window has to correspond to the frequency contents of the eigenfunction to obtain an adequate resolution. A narrow window produces more certainty in the time domain but greater ambiguity in frequency owing to the Heisenberg uncertainty principle (Harris, 1978; Priestley, 1981; Mallat, 2001). The choice of type of window is not critical when applied to the wavelet design. We decided to use a Hanning window.

The resolution in time and frequency of the wavelet transform depends on the spread of the window in time and frequency. This can be measured from the decay of the ambiguity function or from the area of the Heisenberg box (Mallat, 2001). The uncertainty principle proves that this area is a minimum if the window is Gaussian. We applied a Hanning window and this shows the same results. Other window types (Kaiser; Blackman; Triangular; Nuttall) (Priestley, 1981) show slightly worse results. Window optimization requires a more detailed study. It would also depend on the particular data set or whether one desires a better time or frequency resolution.

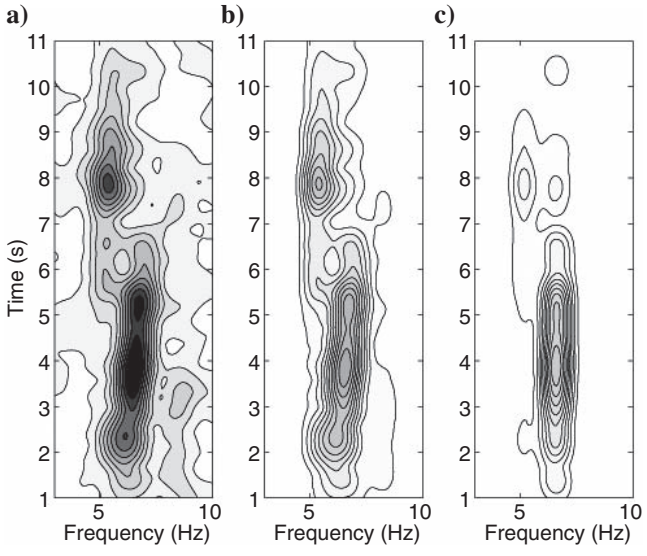

Figure 3. Time-frequency amplitude representation of the signal shown in Figure 1 as a result of applying the adaptive-wavelet transform when: (a) all eigenfunctions were used in the wavelet design, (b) the first 40 eigenfunctions were applied, (c) only the first 10 eigenfunctions were applied.

RESULTS OF ADAPTIVE WAVELETS

In this section, we present representative results to show exactly how the adaptive wavelet method can be applied to different time signals, and we also compare this approach to that of an analysis based on standard wavelets.

Figure 4a represents the first example involving a chirp signal, whose frequency spectrum is shown in Figure 4b. The corresponding time-frequency amplitude representation of this chirp signal, as captured by the two different wavelet methods — by the adaptive wavelet and by the conventional Morlet wavelet — are displayed in Figure 5. The Morlet wavelet was implemented in the frequency domain and adjusted for the same width of the time window.

To adjust our Morlet-wavelet implementation in terms of the frequency and time resolutions, we have used the approach taken by Torrence and Compo (1998). The nondimensional angular scaling frequency was taken as six to satisfy the admissibility condition (Torrence and Compo, 1998). To achieve the very best possible image quality, the following examples have been tested with different scaling powers δj, ranging from 0.5 to 0.001, to cover both large and very small periods to obtain an optimal time-frequency resolution:

$$S_j = s_0 2^{j\delta j}, \quad j = 0,1,2,\ldots, J, \quad J = \delta j^{-1} \log_2(N\delta t/s_0), \tag{15}$$

where s_0 is the smallest resolvable scale; J defines the largest scale (Torrence and Compo, 1998).

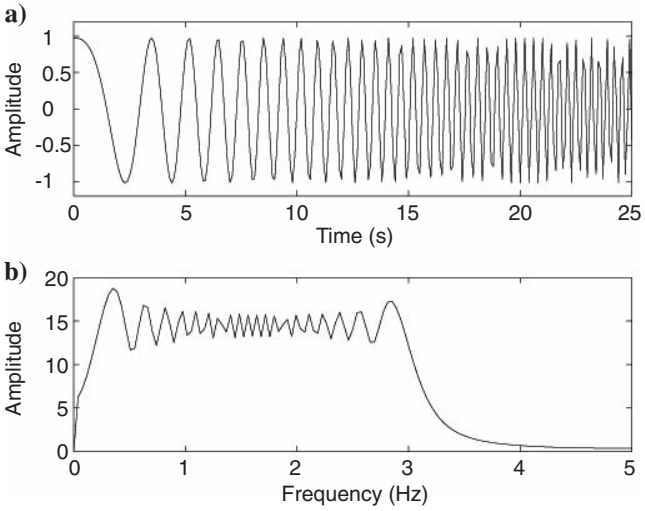

Figure 4. (a) Temporal dependence of the chirp signal; (b) the associated frequency spectrum.

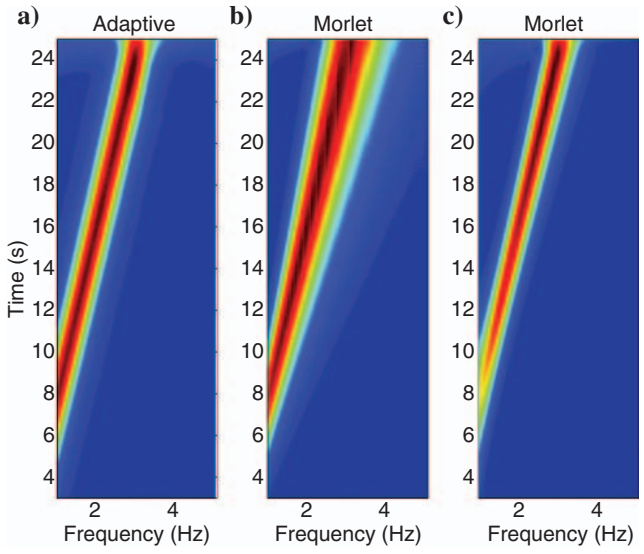

Figure 5. Time-frequency amplitude representation of the chirp signal based upon (a) the adaptive wavelets and (b and c) the Morlet wavelets.

Immediately, we see a much greater fidelity in the result produced by the adaptive wavelet (Figure 5a) in that a nearly perfect ascendance of the frequency content is displayed, in contrast to the broadening of the frequency content with time in the case of the Morlet wavelets (Figure 5b). The amplitude distortion at low frequencies in the Morlet-wavelet result in Figure 5c was an attempt to overcome the broadening effect. We can achieve a nearly constant time-frequency representation in the adaptive-wavelet image by balancing the frequency content of each wavelet function with its time window. Each wavelet function has been assigned its own window, and the width of all windows decreases with increasing frequency.

It is important now to use some synthetic seismic signals to demonstrate the true prowess of our method in simulated geophysical situations. The following two examples test the adaptive-wavelet technique in differentiating various dispersive modes closely spaced or overlapped in time or frequency. These synthetic signals were obtained as a result of forward modeling in the wavenumber domain using the modeling program OSIRIS (Precise Seismic Modeling program) (Odegaard, 2005). The synthetics were designed only for testing purposes.

Figure 6 shows a seismic record that contains four dispersive modes in the frequency ranges as follows: first mode, between approximately 1 and 1.5 Hz; second mode, between 1.5 and 2 Hz; third mode, between 3.2 and 3.5 Hz; and the last mode, between around 3.75 and 4.5 Hz. We note that the last two modes arrive at about the same time. The time-dependence of this wave packet is shown in Figure 6a. The corresponding time-frequency representation of the amplitudes captured by the two wavelets is shown in Figure 7. The clear superiority of the adaptive wavelet method can easily be discerned in Figure 7a in which the four different modes are separated. On the other hand, with the Morlet wavelet, we experienced problems in resolving the two last modes (Figure 7c). Only by sacrificing the time resolution, can we achieve the desirable separation of the modes (Figure 7b). In Figure 7c, two modes seem to be interfering with each other in the time-frequency domain and producing holes in the image. The separation of modes seems to be very critical in our study where a good mode definition is required. We refer to Appendix A for additional comparison between adaptive and Morlet wavelets with more complicated frequency-time contents.

The next example is more complex than the previous one in that we have put the last two modes within the same frequency interval, from about 3.5 to 4.0 Hz, whereas the first two modes are left without changes: first mode within about 1 and 1.5 Hz; and the second, between 1.5 and 2 Hz. This type of signal, shown in Figure 8, brings challenges in separating out the frequency-overlapped modes, the situation which is considered to be the most problematic when analyzing the dispersive surface-wave modes. The superiority of the adaptive wavelets over the Morlet wavelets is more apparent here, as

shown in Figure 9. One can see that the resolution using the adaptive wavelet (Figure 9a) is much better than that using the Morlet-wavelet (Figure 9b and c). The latter images are the result of our best adjustment of the Morlet wavelet in both time and frequency resolution.

The above examples most certainly demonstrate the superiority of the adaptive wavelets over the Morlet wavelets in terms of the clarity of mode separation in the time-frequency plane of the surface-wave signals. This difference is especially poignant in the situation of overlapping modes in both time and frequency domains.

This is an important attribute, because the accuracy of the shear-wave inversion from the group and phase velocities of the surface waves depends on the precise differentiation of the surface-wave modes (Strick, 1959; Hovem et al., 1990; Gaiti et al., 1994; Kuperman et al., 2000; Frivik, 1998; Allnor, 2000; Kritski et al., 2002a). The complexity of the multiscale sedimentary structures manifests itself through the multiscale surface-wave mode patterns. A better technique for image resolution provides us with a hope for a more reliable inversion for the shear properties of marine sediments.

We present next another test with a still more complex time signal, as shown in Figure 10, which consists of six different components (Figure 10a). Also shown is the frequency spectrum (Figure 10b). This signal was produced to imitate the situation when different surface-wave modes intersect at different angles to create potential problems in the resolution.

The time-frequency representation of this complex signal is shown in Figure 11, where it is clear that the adaptive wavelet (Figure 11a) offers a distinct advantage over the Morlet wavelet (Figure

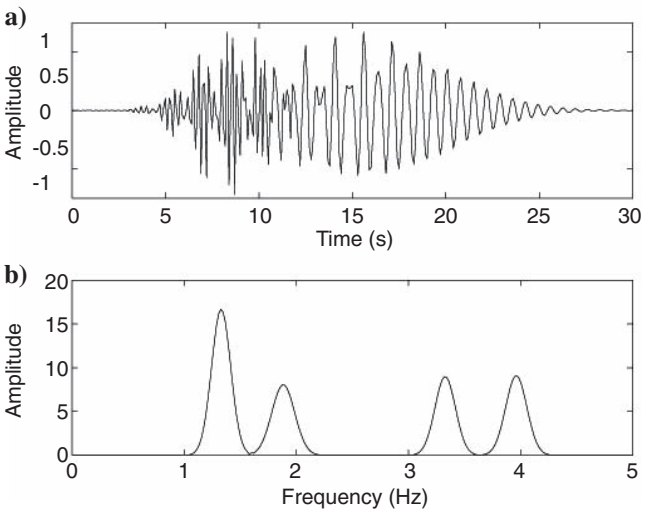

Figure 6. (a) Time representation of the synthetic signal with four modes; (b) the associated frequency spectrum.

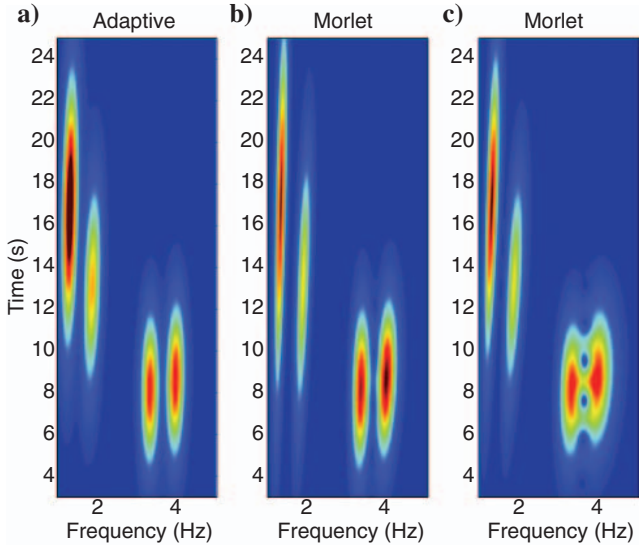

Figure 7. Time-frequency amplitude representation of the synthetic wave packet portrayed in Figure 6. (a) Results from the adaptive-wavelet analysis are presented in comparison with (b) and (c) results from the Morlet-wavelet analysis, where different scaling parameters were used to achieve the best frequency or time representations.

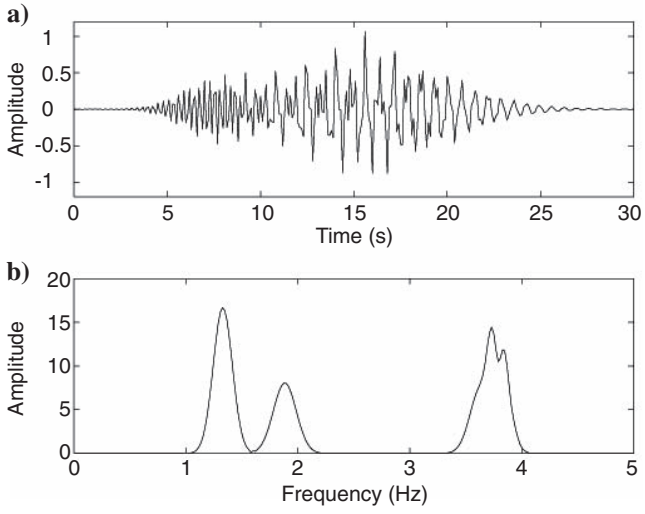

Figure 8. (a) Time representation of the synthetic signal with four modes when two modes overlap in the frequency domain; (b) the associated spectrum.

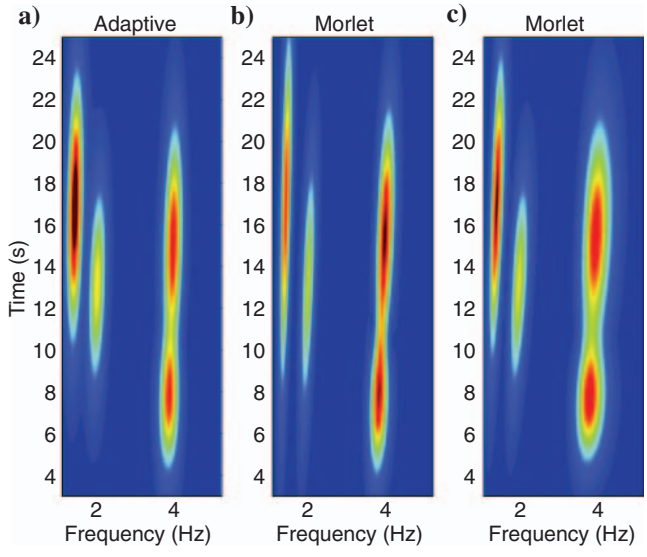

Figure 9. Results of (a) the adaptive-wavelet analysis and (b, c) the Morlet-wavelet analysis for the signal in Figure 8. Different scaling parameters were used for the Morlet wavelets to achieve the best frequency or time representations in (b) and (c).

11b and c) to separate out the intricate morphology produced by the intersection of the various events at different angles. The Morlet-wavelet image in Figure 11b has been produced using our best adjustment in frequency and time resolution. The low-amplitude component at around 25 Hz and between 0.2 and 0.3 s is also present in the Morlet-wavelet time-frequency diagram. However, the amplitudes appear to have been smeared out when the scales are adjusted to get the best frequency resolution (Figure 11b) or very distorted when it is the time resolution that is adjusted (Figure 11c).

In Figure 12, we compare the wavelet analysis of a field record taken from a shallow water survey in the Norwegian shelf (Allnor, 2000). Again, we see that the new adaptive-wavelet approach improves the image quality (Figure 12a) as compared to that of the Morlet-wavelet analysis (Figure 12b and c). This point is especially evident in the high-frequency content, where the image based on the Morlet-wavelet analysis experiences distortions (Figure 12b). These high-frequency distortions, when taken into the interpretation of surface-wave modes, may conceivably cause a less accurate inversion for the group and phase velocities of the surface waves and would consequently give rise to erroneous results in the estimates of the shear-wave velocities.

On the other hand, in Figure 12c (fine scaling for the Morlet wavelet), one can clearly observe distortions in the imaging that, most likely, are related to interference effects between various events. A possible seismic interpretation based on Morlet-wavelet analysis imaging would differ significantly from an interpretation based on the adaptive wavelet.

On the basis of the results of the test examples (Figures 5, 7, 9, and 11), which allow us to compare complex signals from adaptive-wavelet analysis to those from the Morlet-wavelet analysis, we expect that the interpretation of the real signal, based on the Morlet wavelet, is most likely to have errors. The real signal feature is expected to be much more like the image retrieved with the adaptive wavelet analysis. Such interpretations based on the standard wavelet analysis might lead to erroneous inversion results of the shear velocities from the surface-wave modes.

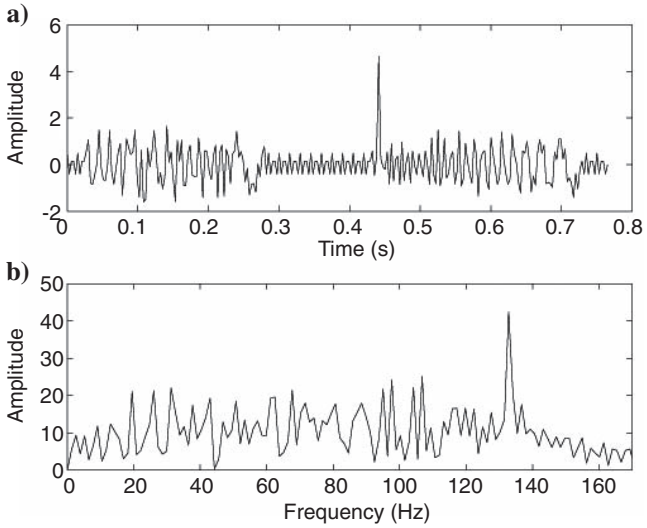

Figure 10. (a) Synthetic signal of the case with six different modes; (b) the associated frequency spectrum.

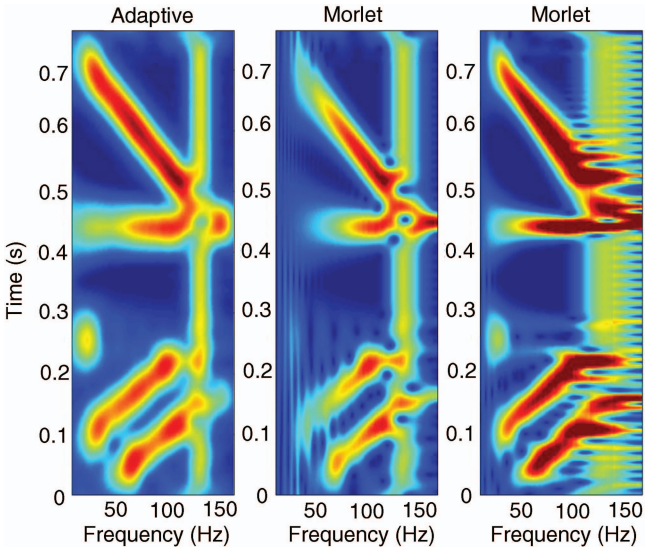

Figure 11. Time-frequency amplitude representation of the complex test signal (shown in Figure 10) from (a) the adaptive wavelets and (b) and (c) the Morlet wavelets, where different scaling parameters were used to achieve the best frequency or time resolution.

DISCUSSION

The developed adaptive method differentiates very efficiently between the coherent and noncoherent parts of the signal. Hence, it is very stable with respect to the noncoherent noise. On the other hand, there are geophysical situations in which the noise and the signal are correlated, as in ground rolls or multiples of reflectors. In this case, a signal-to-coherent-noise ratio is extremely sensitive to the number of eigenfunctions taken into play. This ratio increases with fewer eigenfunctions. But, employing fewer eigenfunctions in the analysis would concomitantly decrease the resolution and the accuracy of the

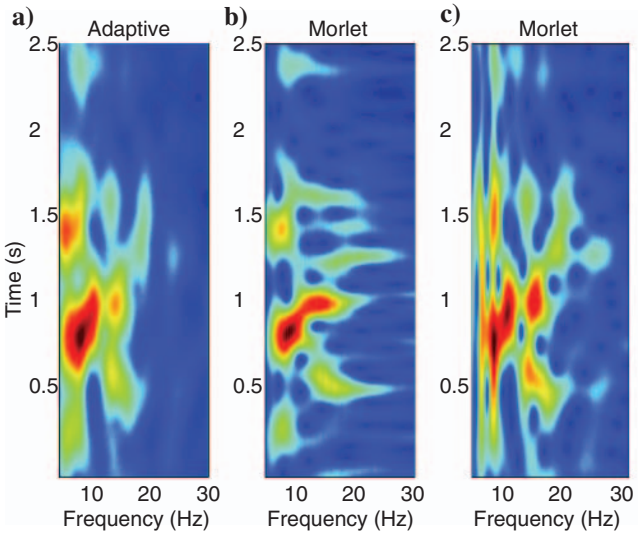

Figure 12. Example of the field seismic record processed with (a) the adaptive wavelets and (b) and (c) the Morlet wavelets, where different scaling parameters were used to achieve the best time or frequency.

final images. Therefore, a trade-off exists between the minimum number of eigenfunctions that would effectively suppress the coherent noise and reasonable quality of the final image. An automatic thresholding of the wavelet energy makes it potentially possible to differentiate certain signal events from noise in situations where the time-frequency structure of these events is known or predictable. The energy threshold can be achieved by selecting a desirable number of the eigenfunctions corresponding to the required energy level for constructing the appropriate adaptive-wavelet scheme. This would selectively remove the low-amplitude areas of the wavelet field that represent noise and, thus, help to differentiate single events from the noise. This technique would be equivalent to a temporal filtering for all frequencies simultaneously, similar to filtering in the standard wavelet-transform field (Torrence and Compo, 1998).

Finally, although the KL transform provides the optimal decomposition of the signal in the sense of minimizing the average approximation error, we have not yet optimized the procedure of mapping eigenfunctions to the wavelet space, and this might result in some degree of nonuniqueness in the wavelet basis set. In the future, we aim to solve this optimization problem in our quest for a set of optimal data-driven wavelets. The potential use of frames (Daubechies, 1992) may also improve the convergence of this adaptive approach.

CONCLUSIONS

In this work, we develop the process for creating a novel class of wavelets that are naturally adapted to the input multiscale time series because their selection is based on statistical estimations of all relevant scales present in the input signal. The method developed here performs better imaging than standard wavelets in decomposing the complex spectra when uncorrelated noise is present and also when modes overlap in time and frequency. The method is more general than the traditional wavenumber-frequency spectrum and can be employed in a laterally heterogeneous physical domain.

In a sense, this adaptive technique defines a statistical signature of the physical phenomenon being investigated. In the case of surface-wave studies, this represents the propagational properties of the surface waves.

ACKNOWLEDGMENTS

The authors thank Yuri Podladchikov (University of Oslo), Lasse Amundsen (Statoil Research Centre, Trondheim), and Maarten De Hoop (Purdue University) for fruitful discussions. Statoil ASA is gratefully acknowledged for permission to publish this work. Dave Yuen was supported by the CMG and the ITR programs of the National Science Foundation. Finally, we thank three anonymous referees and the associate editor Eric Verschuur for their perceptive comments, which have greatly helped to focus and improve this manuscript.

LIST OF SYMBOLS

x_i = Input single time discrete signal
$\mathbf{X}(t)$ = Delay matrix
τ = Time delay
$m_f; m_p$ = Future and past coordinates
Δt = Time sample interval
$\mathbf{\Phi}_{ij}$ = Covariance (correlation) matrix
$z(t)$ = Principal component
$\mathbf{\psi}_i(X)$ = Eigenfunction
λ_i = Eigenvalue
ξ_m = Eigenfunction
ζ_m = Adaptive-wavelet function
$\nu(\lambda_i)$ = Time window function
l = Time window width
$\mathbf{K}_{(l,k)}$ = Global covariance matrix

APPENDIX A

ADDITIONAL ANALYSIS

In this appendix, we will provide an additional comparative analysis on the ability of the adaptive and Morlet wavelets to resolve time series of a complex event. Our special focus is on testing the event interference phenomenon in the time-frequency space (Figure 7c) which, in our opinion, causes distortion holes in the Morlet-wavelet images (Figures 7c and 12c). Figures A-1–A-4 represent various complex signals and their time-frequency representations after the adaptive and Morlet wavelets were applied. Scaling for the Morlet wavelet was adjusted to obtain the best image resolution in time or in frequency. In the example displayed in Figure A-4b, a nondimensional angular frequency was changed to achieve a smooth transition of the wavelet amplitudes. Note that the Morlet wavelet yields a very good separation of events in frequency (Figure A-4b). However, such a good resolution in frequency is achieved at the cost of deteriorating time resolution. An attempt to improve time resolution results in producing artificial holes in the images (Figure A-4c). The cause of this problem lies in the time-frequency mapping of the Morlet wavelet that focuses energy on each chosen central frequency (for each of the scaling periods). This is why the energy image is concentrated around the chosen frequencies only. If, for example, an event occurs at a frequency between f_1 and f_2 and if the scaling period s has a corresponding frequency $f_s \approx 1/s$ which is closer to f_1, the

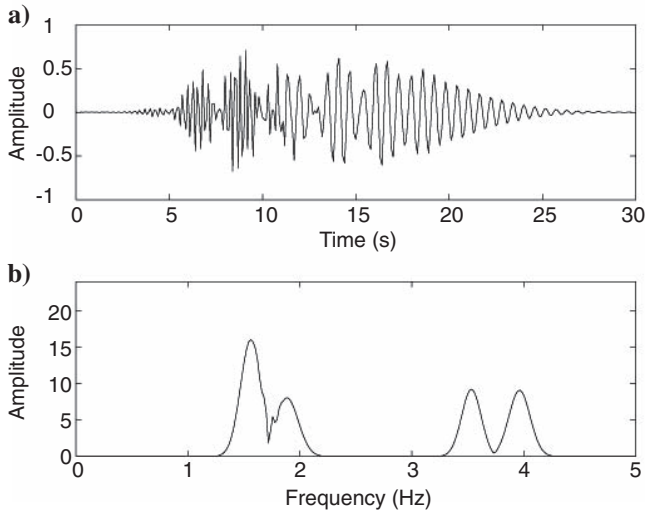

Figure A-1. (a) Synthetic signal of the complex time signal with two modes that are close in frequency and arrive at the receiver at the same time, and (b) the associated frequency spectrum. This figure is based on the signal in Figure 6.

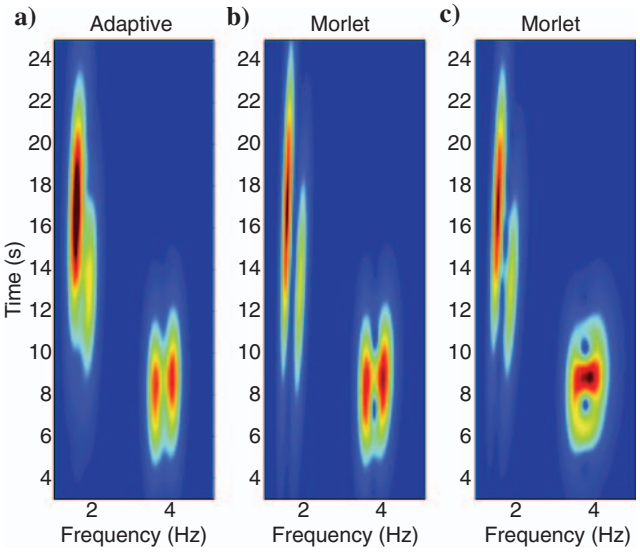

Figure A-2. Results of (a) the adaptive-wavelet analysis and (b, c) the Morlet-wavelet analysis for the signal shown in Figure A-1. For the Morlet wavelet, different scaling parameters were used to achieve the best frequency and time representations in (b) and (c).

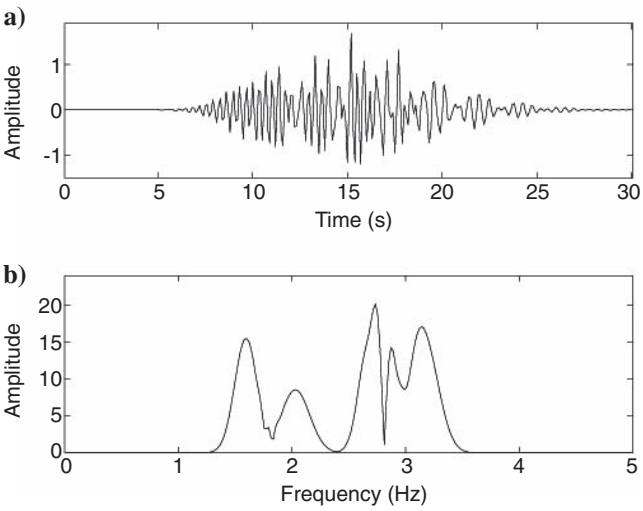

Figure A-3. (a) Synthetic complex signal of the case with five modes; (b) the associated frequency spectrum.

energy of this event will be attributed to the f_1 bin. Nothing in the frequencies between f_1 and f_2 is available for collecting signal energy. In principle, it is possible to choose the scaling so accurately that it would fall exactly into or very close to the predefined central frequency (of corresponding scale), thus providing very small gaps in frequency-defined bins and making imaging smoother. However, this would require a good preliminary knowledge of the time-frequency structures of the events and absolutely is not possible. On the other hand, for the adaptive wavelet, we applied a frequency-contribution scheme when the frequency content from different eigenmodes is collected and sorted out for all frequencies. This redistribution of energy makes time-frequency mapping smoother and does not produce holes in images.

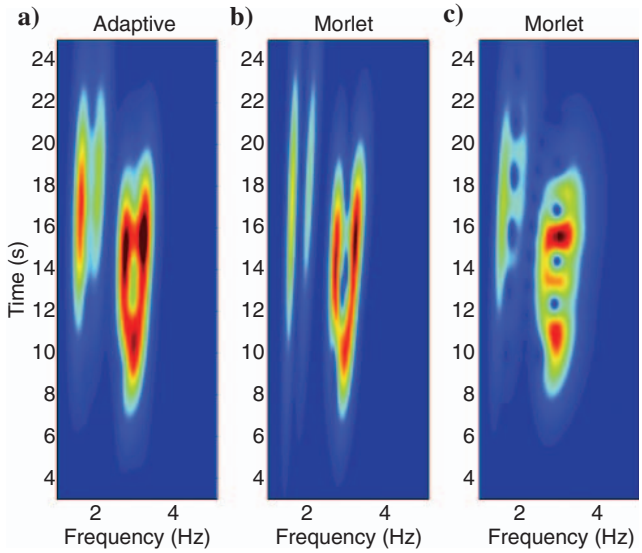

Figure A-4. Results of (a) the adaptive-wavelet analysis and (b, c) the Morlet-wavelet analysis for the signal shown in Figure A-3. For the Morlet wavelets, different scaling parameters were used to achieve the best frequency or time representations in (b) and (c).

REFERENCES

Abbate, A., C. M. DeCusatis, and P. K. Das, 2002, Wavelets and subbands, fundamentals and applications: Birkhäuser Verlag.

Aki, K., and P. Richards, 2002, Quantitative seismology, 2nd ed.: University Science Books.

Allnor, R., 2000, Seismo-acoustic remote sensing of shear wave velocities in shallow marine sediments: Doktor Ingenior thesis, The Norwegian University Science and Technology.

Aster, R. C., B. Borchers, and C. H. Thurber, 2005, Parameter estimation and inverse problems: Elsevier Academic Press.

Bendat, J., and A. Piersol, 1980, Engineering applications of correlation and spectral analysis: John Wiley & Sons, Inc.

Biot, M. A., 1952, Propagation of elastic waves in cylindrical bore containing a fluid: Journal of Applied Physics, **23**, 997–1005.

Bodet, L., K. van Wijk, A. Bitri, O. Abraham, P. Côte, G. Grandjean, and D. Leparoux, 2005, Surface wave inversion limitations from laser-Doppler physical modeling: Journal of Environmental & Engineering Geophysics, **10**, 151–162.

Broomhead, D. S., and G. P. King, 1986, Extracting qualitative dynamics from experimental data: Physica D **20**, 217–236.

Chui, C. K., 1992, Wavelet analysis and its applications, *in* Wavelets: A tutorial in theory and applications, vol. 2: Academic Press.

Coifman, R. R., Y. Meyer, and V. Wickerhauser, 1992, Wavelet analysis and signal processing, *in* M. B. Ruskai et al., eds., Wavelets and their applications: Jones & Barlett Publishers, 153–178.

Daubechies, I., 1992, Ten lectures on wavelets: CBMS-NSF Regional conference series in applied mathematics.

Dziewonski, A. M., S. Bloch, and M. Landisman, 1969, A technique for the analysis of transient seismic signals: Bulletin of the Seismological Society of America, **57**, 427–444.

Frivik, S. A., 1998, Determination of shear properties in the upper seafloor using seismo-acoustic interface waves: Ph.D. thesis, Norwegian University of Technology.

Gabor, D., 1946, Theory of communication: Journal of Institute of Electrical Engineers, **93**, 429–457.

Gaiti, A., A. Tuncay, and R. Stoll, 1994, Estimation of shear wave velocity in shallow marine sediments: IEEE Journal of Oceanic Engineering, **19**, 58–72.

Gibson, J. F., J. D. Farmer, M. Casdagle, and S. Eubank, 1992, An analytical approach to practical state space reconstruction: Physica D, **57**, 1–30.

Golub, G., and C. Van Loan, 1983, Matrix computations: North Oxford Academic.

Goupillaud, P., A. Grossmann, and J. Morlet, 1984, Cycle octave and related transforms in seismic signal analysis: Geoexploration, **23**, 85–102.

Grossmann, A., and J. Morlet, 1984, Decomposition of Hardy functions into square integrable wavelets of constant shapes: SIAM Journal of Mathematical Analysis, **15**, 723–736.

Harris, F. J., 1978, On the use of windows for harmonic analysis with the discrete Fourier transform: Proceedings of the IEEE, 66, 51–83.
Haskell, N. A., 1953, The dispersion of surface waves in multilayered media: Bulletin of the Seismological Society of America, **43**, 17–34.
Haykin, S., ed., 1991, Advances in spectrum analysis and array processing, vol. 1: Prentice Hall Advanced Reference Series.
Helstrom, C. W., 1968, Statistical theory of signal detection: Pergamon Press, Inc.
Hogan, J., and J. Lakey, 2005, Time-frequency and time-space methods. Adaptive decompositions, uncertainty principles and sampling: Birkhaüser-Verlag, Applied and Numerical Harmonic Analysis.
Holschneider, M., 1995, Wavelets and analysis: Oxford Science Publication.
Holschneider, M., R. Kronland-Martinet, J. Morlet, and Ph. Tchamitchian, 1989, A real-time algorithm for signal analysis with the help of the wavelet transform: Springer-Verlag, Berlin.
Hovem, J., M. D. Richardson, and R. Stoll, eds., 1990, Shear waves in marine sediments: Kluwer Academic Press.
Kaiser, G., 1994, A friendly guide to wavelets: Birkhäuser-Verlag.
Karhunen, K., 1947, Zur spektralttheorie stochastischer prozesse: Annales Academiae. Scientiarum Fennicae, A1, Mathematica-Physica, **34**, 1–7.
Kritski, A., D. A. Yuen, and A. P. Vincent, 2002a, Properties of near surface sediments from wavelet correlation analysis: Geophysical Research Letters, **29**, 1922, doi:10.1029/2001GL014592.
———, 2002b, The physical properties of marine sediments as inferred from wavelet correlation analysis: Electronic Geosciences, 7, 1–23.
Kumar, P., and E. Foufoula-Georgiou, 1997, Wavelet analysis for geophysical applications: Reviews of Geophysics, **35**, 385–412.
Kuperman, W. A., F. Jensen, M. Porter, and H. Schmidt, 2000, Computational acoustics, modern acoustic and signal processing: Springer-Verlag.
Loeve, M. M., 1955, Probability theory: D. Van Nostrand Co.
Mallat, S. A., 2001, Wavelet tour of signal processing: Academic Press, Inc.
OSIRIS, 2005, Precise seismic modelling: Odegaard A/S.
Packard, N. H., J. P. Crutchfield, J. D. Farmer, and R. S. Shaw, 1980, Geometry from a time series: Physical Review Letters, **45**, 712–716.
Poiree, B., and F. Luppe, 1991, Evanescent plane waves and the Scholte-Stoneley interface wave: Journal Acoustique, **4**, 575–588.
Potty, G. R., J. Miller, and J. F. Lynch, 2003, Inversion for sediment geoacoustic properties at the New England Bight, part 1: Journal of the Acoustical Society of America, **114**, 1874–1887.
Priestley, M. B., 1981, Spectral analysis and time series: vol. 2: Multivariate series, prediction and control: Academic Press, Inc.
Riesz, F., and B. Sz. -Nagy, 1955, Functional analysis: Frederick Ungar Publ. Co.
Strick, E., 1959, Propagation of the elastic wave motion from an impulsive source along a fluid/solid interface. III. The pseudo-Rayleigh wave: Philosophical Transactions of the Royal Society of London. Series A, Mathematical and Physical Sciences, **251**, 455–523.
Torrence, C., and G. P. Compo, 1998, A practical guide to wavelet analysis: Bulletin of the American Meteorological Society, **79**, 61–78.
Vautard, R., and M. Ghil, 1989, Singular spectrum analysis in non-linear dynamics, with applications to paleoclimatic time series: Physica D, **35**, 395–424.
Yiou, P., D. Sornette, and M. Ghil, 2000, Data-adaptive wavelets and multiscale singular-spectrum analysis: Physica D, **142**, 254–290.
Yuen, D. A., G. Erlebacher, O. V. Vasilyev, D. E. Goldstein, and M. Fuentes, 2004, Role of wavelets in physical and statistical modeling of complex geological processes: Pure and Applied Geophysics, **161**, 2231–2244.
Yuen, D. A., A. P. Vincent, M. Kido, and L. Vecsey, 2002, Geophysical applications of multidimensional filtering using wavelets: Pure and Applied Geophysics (PAGEOPH), **159**, 2285–2309.